Stripe patterns for Gierer-Meinhard model in thin domains

Theodore Kolokolnikov[a1], Leila Mohammadi[1], and David Iron[1]

[1] *Department of Mathematics and Statistics, Dalhousie University Halifax, Nova Scotia, B3H3J5, Canada*

We expore pattern formation for the GM model on thin domains. If the domain is sufficiently thin, the pattern consists of a stripes which are nearly one-dimensional. We analyse patterns consisting of one, two or many stripes. We find that a single stripe can be located either at the thickest or thinnest part of the channel, depending on the choice of parameters. In the limit of many stripes, we derive an effective pattern density description of the equilibrium state. The effective density is easily computable as a solution of a first order ODE subject to an integral constraint. Depending on problem parameters, the resulting pattern can be either global spanning the entire domain, or can be clustered near either thickest or thinnest part of the domain. In addition, instability thresholds are derived from the continuum density limit of many stripes. Full two-dimensional numerical simulations are performed and are shown to be in agreement with the asymptotic results.

1. INTRODUCTION

In this paper we explore pattern formation for Gierer-Meinhardt (GM) model on thin domains. The standard GM model is [1, 2]:

$$a_t = \varepsilon^2 \Delta a - a + a^p/h^q, \qquad 0 = d^2 \Delta h - h + a^m/h^s, \tag{1}$$

and, as with most of studies of this model, we assume that the activator a diffuses much slower than the inhibitor h, so that $\varepsilon \ll d$. As is well known, in this regime the solution consists of spikes (localized concentrations, or spots) that exhibit a wide variety of phenomena that have been intensively studied over the last 3 decades. We refer the reader to books [3, 4] and references therein. Similar spot patterns have been studied in many other reaction-diffusion models. Some prominenet examples include Gray-Scott model [5–9] the Schankenberg model [10–12], vegetation patches in arid environments [13–18], a model of crime hot-spots in a model of residential burglaries [19–22] and animal skin patterns, [23–25].

One of the key results going back to [2, 26] is that the parameter d can be used to tune the number of spikes: increasing d can trigger the so called competition or coarsening instability threshold, which decreases the total number of spikes; the maximum allowed number of spikes is a decreasing function of d. Similar thresholds exist in other models as well [9, 11, 21] and in more general contexts, such as in the presence of precursor [27–29] or spatial heterogeneity [30, 31].

Here, we study spike dynamics and stability for the GM model inside thin channels. See Figures 1,2,4 for examples. We are interested in the regime where the pattern is quasi-one-dimensional, in the sense that the concentration of either activator or inhibitor is nearly constant in the direction that is perpendicular to the channel. We will refer to such a pattern interchangeably as a stripe or a spike. In particular, stripes occur when the channel cross-sectional thickness is of $O(\varepsilon)$: when the domain is too thick, the stripe will break up into spots [32–36].

In the case where domain is very thin in one direction, a standard reduction – see Appendix C – results in a one-dimensional version of the GM model, but with an additional inhomogeneous drift term which encodes the cross-sectional area along the domain. This reduction results in the the modified diffusion operator as follows:

$$\Delta \to \partial_{xx} + \frac{A'(x)}{A(x)}\partial_x. \tag{2}$$

Here, x denotes the arclength coordinate along the boundary of the channel, and $A(x)$ is the cross-sectional length of the domain at location x, and is assumed to be small. For convenience, we also rescale $a = \hat{a}\varepsilon^e, h = \hat{h}\varepsilon^f$ with $e = -1/\left(m - (1+s)\,(p-1)/q\right), \quad f = -1/\left(mq/(p-1) - (1+s)\right)$, so that after dropping the hats the GM model becomes

$$a_t = \varepsilon^2 \left(a_{xx} + \alpha(x) a_x\right) - a + a^p/h^q, \tag{3a}$$

$$0 = d^2 \left(h_{xx} + \alpha(x) h_x\right) - h + \frac{1}{\varepsilon} a^m/h^s \tag{3b}$$

[a] Corresponding author: tkolokol@gmail.com

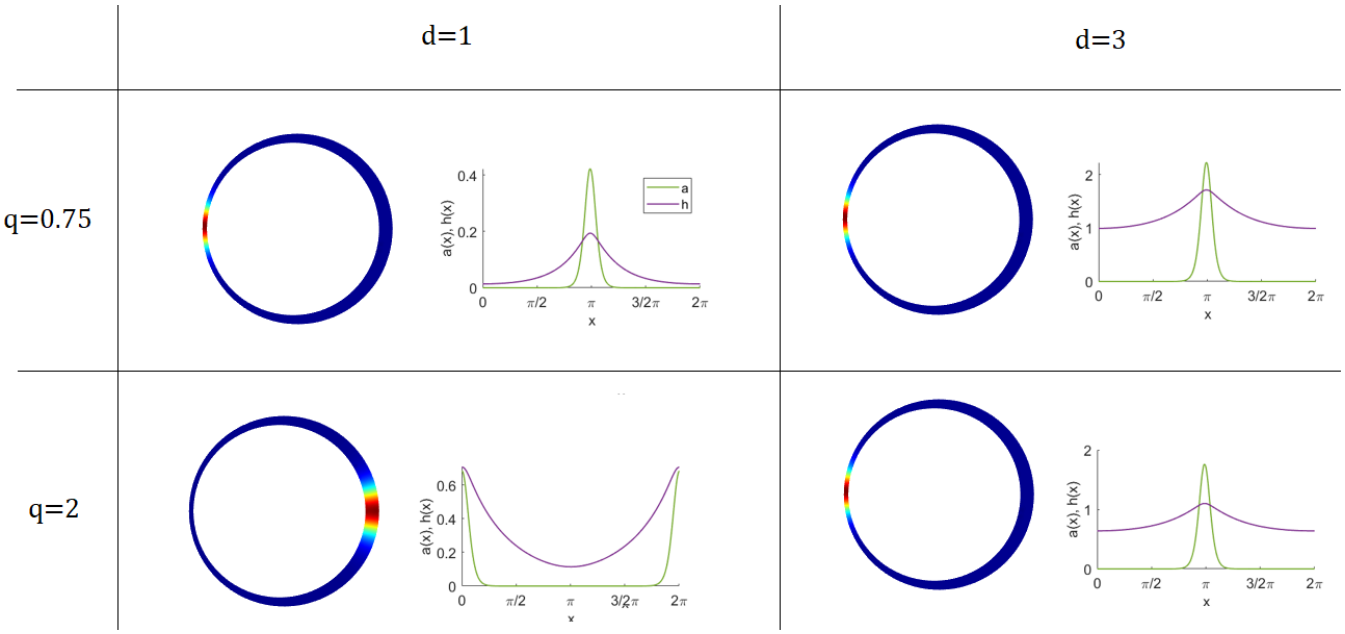

FIG. 1. Stable equilibrium solutions of the full 2D system (1) consisting of a single spike inside an annular region of uneven thickness. The outer boundary is unit circle. The inner boundary is a circle which is at a minimum distance of 0.05 and a maximum distance of 0.15 from the outer boundary. Full 2D time-dependent problem was solved using an initial condition consisting of a single spike at $x = \pi/2$. Snapshots show the solution after it converged to a (stable) equilibrium. Parameters d and q are as shown, while other parameters are $\varepsilon = 0.1$, $p, m, s = 2, 2, 0$. Note that the spike is expected to be stable at the thinnest part of the domain when d is large, regardless of q. When d is small, the spike is stable at the thinnest part if $q < p - 1$, but is stable at the thickest part when $q > p - 1$.

with $\alpha = A'/A$. The presence of inhomogeneities $\alpha(x)$ in both a and h equations introduces novel features to the GM model, and the rest of the paper is dedicated to the study of these. A similar model in the context of a convective flow for the Schnakenberg model, but with a constant α, was studied in [12].

Throughout this paper, for concreteness we will take the domain such as shown in Figure 1. It is a region whose outer boundary is a unit circle, and whose inner boundary is an off-center circle such that minimum and maximum distance from the outer boundary is $d_{\min}$ and $d_{\max}$, respectively, with $d_{\min} \le d_{\max} \le O(\varepsilon) \ll 1$. We will assume that the inner circle is closest to the outer circle on the left. In the limit $d_{\min}, d_{\max} \ll 1$, we find the corresponding $\alpha(x)$ to be

$$\alpha(x) \sim \frac{1}{2} \frac{-\left(\kappa^2 - 1\right) \sin x}{1 + \kappa^2 + \left(\kappa^2 - 1\right) \cos x}; \quad \kappa = d_{\max}/d_{\min} \tag{4a}$$

(see Appendix C) where $x = \theta$ is the arclength coordinate along the outer circle. The equations (3) are then posed on $x \in [0, 2\pi]$ with periodic boundary conditions. For concreteness, we will fix

$$\kappa = 3 \tag{4b}$$

for the remainder of the paper; the graph of the resulting $\alpha(x)$ is illustrated in Figure 2(c).

Figures 1,2,4 illustrate main results. We study either a single stripe, a configuration involving two stripes, and N stripes where N is large. We are primarily concerned with stripe locations. For large N, we also recover instability thresholds as a function of d (Proposition 3.2). We compute asymptotic stripe locations for 1 or 2 stripes, as well as effective density distribution for N spikes. It turns there are two distinct regimes: the location as well the extent of a cluster changes depending on whether $q < p - 1$ or $q > p - 1$. The "standard" parameter set $(p, q, m, s) = (2, 1, 2, 0)$ is on the boundary $q = p - 1$ and is exceptional in that sense.

2. REDUCED SYSTEM; ONE OR TWO STRIPES

We consider a solution consisting of N stripes, as illustrated in Figure 4. Let $x_k(t)$ denote the stripe location along the channel. This location changes slowly in time. In Appendix A, we use the standard quasi-steady-state

approximation to derive the following system of algebro-differential equations for evolution of spike centers x_k, coupled with heights $V_k \sim h(x_k)$. We summarize the result as follows.

Proposition 2.1. *In the limit $\varepsilon \ll d$, a quasi-equilibrium solution to (3) consisting of N stripes has the form*

$$a(x,t) \sim \sum V_j^{q/(p-1)} w\left(\frac{x - x_j(\varepsilon^2 t)}{\varepsilon}\right), \tag{5}$$

$$H(x,t) \sim b_m \sum_j V_j^{\gamma} G\left(x, x_j\right) \tag{6}$$

where $w(y)$ is a standard ground state solution which satisfies

$$w_{yy} - w + w^p = 0; \quad w'(0) = 0; \quad w\left(y\right) \to 0 \text{ as } y \to \pm\infty, \tag{7}$$

the constant b_m is given by

$$b_m = \int_{-\infty}^{\infty} w^m(y) dy, \tag{8}$$

$G(x,\xi)$ is the Green's function satisfying

$$d^2\left(G_{xx} + \alpha(x) G_x\right) - G = -\delta(x-\xi), \tag{9}$$

and $x_j(t\varepsilon^2)$ is the time-dependent location of j-th stripe which is coupled to weights V_j and solves the following differential-algebraic system:

$$x_k' = -\alpha(x_k) - 2b_m \frac{q}{p-1} \frac{1}{V_k} \sum_j V_j^{\gamma} G_x(x_k, x_j) \tag{10a}$$

$$V_k = b_m \sum_j V_j^{\gamma} G(x_k, x_j); \tag{10b}$$

$$\gamma = \frac{qm}{p-1} - s; \tag{10c}$$

where $G_x(x_k, x_k) = \frac{1}{2}\left(G_x(x_k^+, x_k) + G_x(x_k^-, x_k)\right)$.

Note how the thickness $\alpha(x)$ of the domain appears in both the Green's function (9) as well as in equation (10). For a general $\alpha(x)$ and d, the Green's function equation (9) does not have an explicit solution. However in the limits of large or small d, further asymptotics are possible. We now consider one and two-stripe configurations.

Single stripe. We begin by considering a single stripe, whose center we denote by x_0. In this case, equations (10) reduce to

$$x_0' = -\alpha(x_0) - 2\frac{q}{p-1} \frac{G_x(x_0, x_0)}{G\left(x_0, x_0\right)}. \tag{11}$$

First, suppose d is sufficiently large. This is the so-called near-shadow limit [37]. In this case it is easy to show that $\frac{G_x(x_0,x_0)}{G(x_0,x_0)} = O(d^{-2})$, so that $-\alpha(x)$ in (11) is dominant and we obtain

$$x_0' \sim -\alpha(x_0), \quad d \gg 1 \tag{12}$$

Consequently, equilibrim location for x_0 then correspond to zeros of $a = A'/A$, with *stable equilibrium corresponding to the minimum* of cross-sectoional area $A(x)$.

Next, we consider the case of small d. We use WKB techinques to estimate G in this case – see Appendix B, equations (46), (47). As a result, we obtain the following equation of motion for a single spike:

$$x_0' \sim \left(-1 + \frac{q}{p-1}\right) \alpha(x_0), \quad d \ll 1. \tag{13}$$

Equations (12) and (13) show that in the cases of d either small or large, the equilibria locations $x_0' = 0$ correspond to zeros of $\alpha\left(x\right) = A'(x)/A(x)$, but their stability can *switch* depending on the sign of $q + 1 - p$: if $p > q + 1$, stable equilibria correspond to the minimum of A, and unstable to the maximum of A; this is reversed when $p < q + 1$.

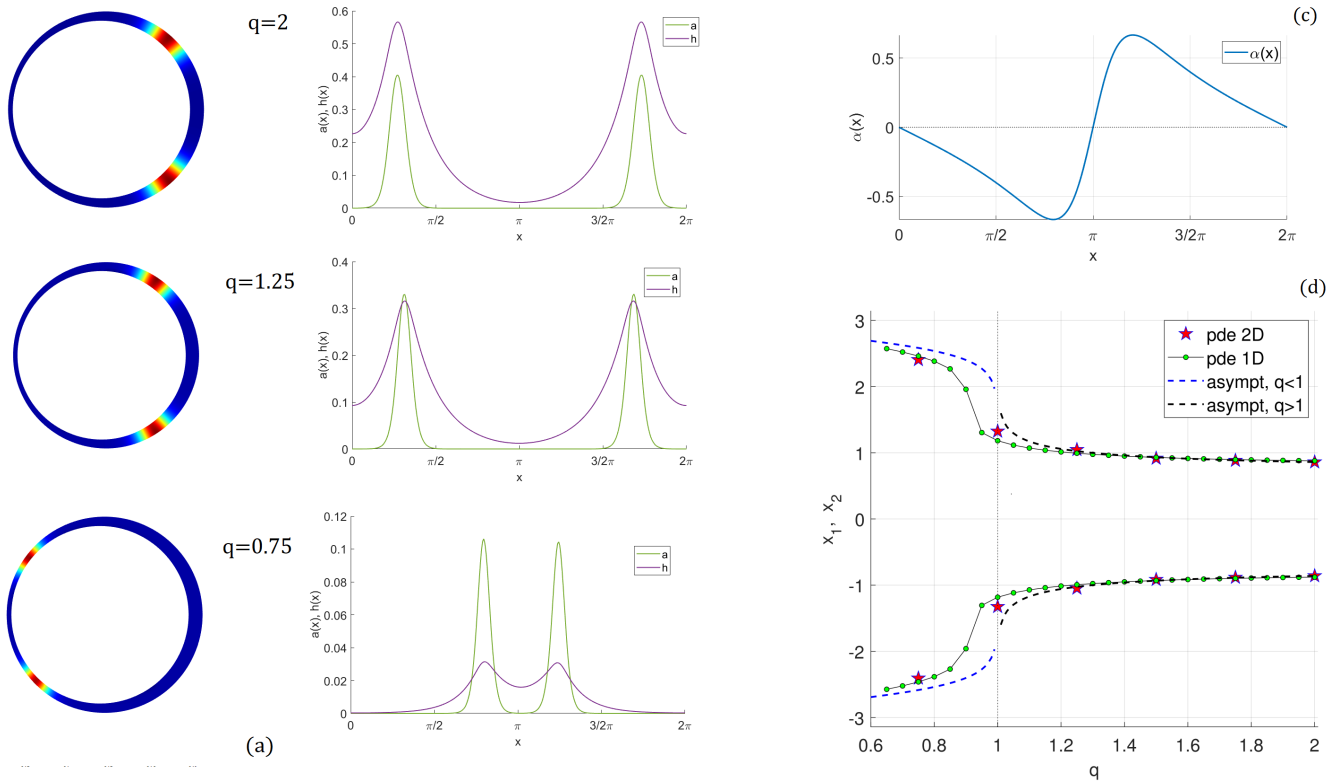

FIG. 2. Two spikes inside an annular region of uneven thickness. The outer boundary is unit circle. The inner boundary is the a circle through points $-1+0.05$, $1-0.15$ (i.e. $\kappa=3$ in (4)). The first column shows the equilibrium state for the full 2D system (1). Second column shows the corresponding equilibrium in the 1D system (3), approximating the solution along the boundary of the domain. (a-c) Parameter values are $\varepsilon=0.07$, $D=0.2$, $p,m,s=2,2,0$, and with q as indicated. (c) The sketch of $\alpha(x)$ given by (4) with $\kappa=3$, which was used in computations of the second column. (d) Equilibrium spike positions as a function of q for two-spike configurations; other parameters as in (a). Curve "pde 2D" is obtained by simulating the full 2D problem (1). Curve "pde 1D" simulates the reduced 1D problem (3). Curve "asympt $q<1$" is the spike locations as given by Proposition 2.2 with expansion near $x_0=\pi$. Curve "asympt $q>1$" is the expansion near $x_0=0$.

The four cases ($q \lessgtr p-1$, d large or small) are illustrated in Figure 1. Interestingly, the case $p=q+1$ (which includes the so-called "standard" GM exponents $p=2, q=1$) is on the boundary $q=p-1$: higher-order analysis (outside the scope of this paper) would be required to analyse the dynamics of a single spike in this case.

Two symmetric stripes. Figure 2 illustrates our results for symmetric configurations consisting of two stripes. Here, we only consider the case where d is asymptotically small, and the two stripes are symmetrically located with respect to domain as shown in Figure 2: either near the minimum or the maximum (when d is large, two spikes are unstable due to a competition instability).

More generally, suppose that the channel has a reflection symmetry with the axis of reflection perpendicular to the channel. We will then look for a two-stripe symmetric solution close to the axis of symmetry. Take x to be transversal coordinate with $x=0$ located at the symmetry point. Then $A(x)$ is an even function so that $\alpha(x)$ is odd. We look for a symmetric solution with respect to $x=0$. Setting $r=x_1=-x_2$ and $V_1=V_2$, equations (10) then become

$$r' = -\alpha(r) - 2\frac{q}{p-1}\frac{G_x(r,r)+G_x(r,-r)}{G(r,r)+G(r,-r)}.$$

For small d, we use the WKB approximation (48), (49) to estimate

$$\frac{G_x(r,r)+G_x(r,-r)}{G(r,r)+G(r,-r)} \sim \frac{-\frac{1}{2}\beta(r)+\exp\left(-\frac{2r}{d}\right)\left(-\frac{1}{d}-\frac{1}{2}\beta(r)\right)}{1+\exp\left(-\frac{2r}{d}\right)}.$$

so that

$$r' \sim \frac{\frac{2q}{p-1}\frac{1}{d}\exp\left(-\frac{2r}{d}\right)}{1+\exp\left(-\frac{2r}{d}\right)} + \alpha(r)\left(-1+\frac{q}{p-1}\right). \tag{14}$$

In the case $q = p-1$, the term having α completely disappears from the equation. In this case the two spikes locally repel each other regardless of the choice of α, and there is no equilibrium near $r = 0$.

More generally, we seek a steady state of (14) for small r. We may then expand in Taylor series $\alpha(r) \sim r\alpha'(0)$, so that (14) becomes

$$r' \sim \frac{\frac{2q}{p-1}\frac{1}{d}\exp\left(-\frac{2r}{d}\right)}{1+\exp\left(-\frac{2r}{d}\right)} + r\alpha'(0)\left(-1+\frac{q}{p-1}\right). \tag{15}$$

The steady state with r small exists and is stable with respect to the ODE (15) if and only if $\alpha'(0)(q-p-1) < 0$. We summarize as follows

Proposition 2.2. *Suppose that $\alpha(x)$ has a root at $x = x_0$ and suppose that $\alpha'(x_0)(q-p-1) < 0$. Then there is a two-spike steady state with spike positions at $x \sim x_0 \pm r$, where $r = O(d\log d^{-1})$ asymptotes to the small solution of*

$$e^{2r/d} \sim \frac{1}{r}\frac{1}{d}\frac{2q}{\alpha'(x_0)(p-1-q)}. \tag{16}$$

No such solution exists if $q = p-1$ or $\alpha'(x_0)(q-p-1) > 0$,

Figure 2 shows a direct comparison between the full 2D model (1) and its one-dimensional reduction (3) with $\alpha(x)$ given by (4). Note that

$$\alpha'(0) = -\frac{\left(\kappa^2-1\right)}{4\kappa^2} < 0, \quad \alpha'(\pi) = \frac{\left(\kappa^2-1\right)}{4} > 0 \tag{17}$$

Consequently, according to Proposition 2.2, two stripes appear on the right $q > p-1$, and on the left when $q < p-1$. This is confirmed with direct simulations.

3. MANY STRIPES

For more than two spikes, equations of motion (10) and its equilibrium become too complex to solve exactly. However as the number N of spikes increase, it becomes possible to gain insight by looking at the limit of large N, as was done in [28, 29], in the limit $d = O(N^{-1})$. In this section, we use the ideas introduced in [28] to compute the effective spike density in the limit of large N.

Let us first define what we mean by spike density $\rho(x)$. We first sort spike positions in increasing order, $x_1 < x_2 < \ldots < x_N$. As we will show, the typical inter-spike will be of $O(d)$. We therefore introduce a continuous function $x(s)$, $s = 0 \ldots dN$, such that $x_k = x(s)$, where $s = kd$. Finally, define

$$u(x) := x'(s); \tag{18}$$

and note that then $x_{j+1} - x_j \approx u(x_j)d$. The effective density is then defined by $\rho(x) := \frac{1}{u(x)}$ Note that $\rho(x)dx = \frac{1}{x'(s)}\frac{dx}{ds}ds = ds$, so that $\int_a^b \rho(x)dx = s|_a^b$. In particular, $\int_D \rho(x)dx = Nd$, where D is the support of $\rho(x)$.

To obtain a continuum approximation, we shall use the fact that the Green's function decay exponentially fast for small d, which makes it possible to simplify the sums in (10). Let $j = k + l$ and expand

$$x_k = x(s) = x;$$
$$x_j = x(s+dl) = x(s) + dlx'(s) + d^2\frac{l^2}{2}x''(s) + \ldots.$$

We then estimate $x''(s) = u_x u$ so that

$$x_k = x; \qquad x_j = x + dlu + d^2\frac{l^2}{2}uu_x + \ldots \tag{19}$$

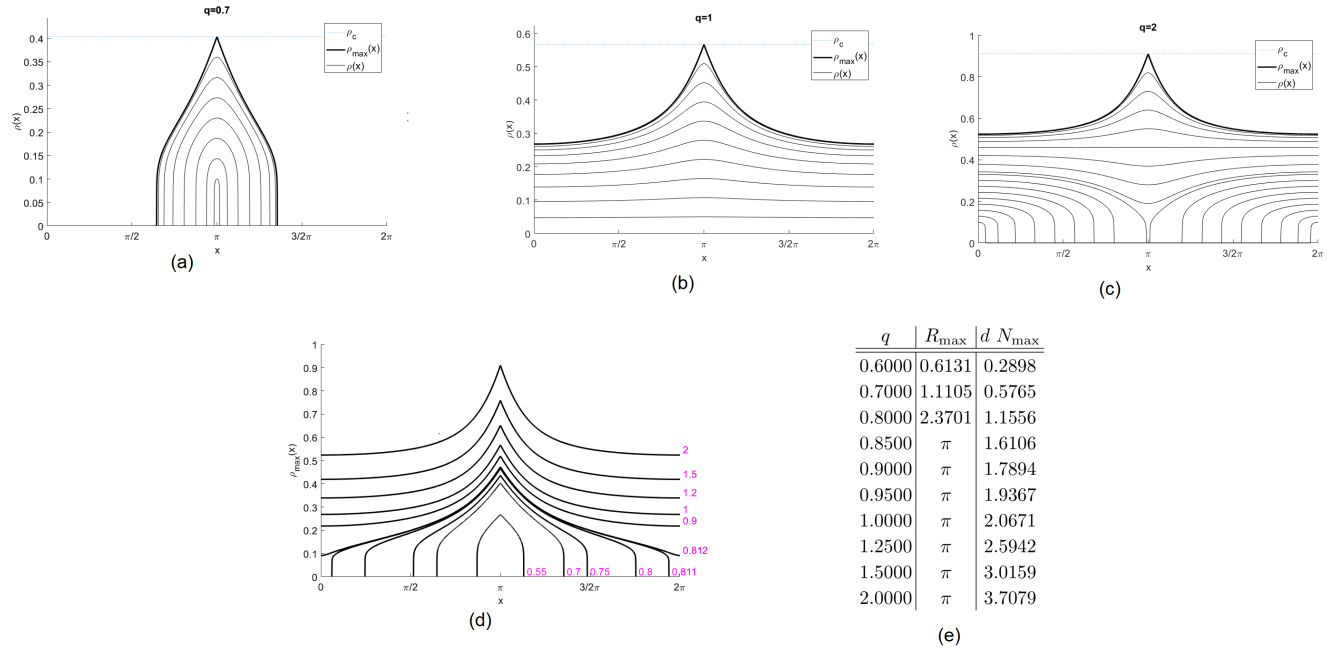

q	$R_{\max}$	$d\ N_{\max}$
0.6000	0.6131	0.2898
0.7000	1.1105	0.5765
0.8000	2.3701	1.1556
0.8500	π	1.6106
0.9000	π	1.7894
0.9500	π	1.9367
1.0000	π	2.0671
1.2500	π	2.5942
1.5000	π	3.0159
2.0000	π	3.7079

FIG. 3. (a-c): Solutions of ODE (21) for the density $\rho(x) = 1/u(x)$ corresponding to different admissable initial conditions (for which $\rho(x) < \rho_c$) with q as indicated, and with $\alpha(x)$ as in (4) and $p = 2, m = 2, s = 0$. (d) Plot of $\rho_{\max}(x)$ as a function of q, other parameters are as in (a-c). (e) $N_{\max}d$ and cluster size $R_{\max}$ as a function of q, see text.

We now expand $\sum_j V_j^\gamma G(x_k, x_j)$. Introduce a continuum variable $V(x)$ with the property that $V_k = V(x_k)$. Using (**??**) we estimate

$$\sum V_j^\gamma G(x_k, x_j) \sim \frac{1}{2d} V^\gamma(x) \sum_{l=-\infty}^{\infty} e^{-|l|u} \sim \frac{1}{2d} V^\gamma(x) \coth(u/2);$$

so that

$$V(x) = \left(\frac{1}{d} \frac{b_m}{2} \coth(u/2) \right)^{\frac{1}{1-\gamma}}. \tag{20}$$

Next, we compute $\sum_j V_j^\gamma G_x(x_k, x_j)$, which requires a two-order expansion due to cancellation at the leading order. We have:

$$2d^2 G_x(x_k, x_j) \sim \operatorname{sign} l e^{-|l|u} + d \left\{ \frac{\beta(x)}{2} \left(|l|\, u - 1 \right) e^{-|l|u} - \frac{l^2}{2} u u_x e^{-|l|u} \right\}$$

$$V_k^\gamma = V^\gamma(x); \quad V_j^\gamma \sim V^\gamma(x) + dlu\gamma V^{\gamma-1}(x) V'(x)$$

so that

$$2d^2 \sum V_j^\gamma G_x \sim d\gamma V^{\gamma-1} V'(x) \sum |l|\, u e^{-|l|u} + dV^\gamma \left\{ \frac{\beta}{2} \sum \left(|l|\, u - 1 \right) e^{-|l|u} - u_x \sum \frac{l^2}{2} u e^{-|l|u} \right\}$$

where all the sums are $\sum = \sum_{l=-\infty}^{\infty}$. We further compute:

$$V^{\gamma-1}(x) = d \frac{2}{b_m} \tanh(u/2);$$

$$V^{\gamma-2} V'(x) = d \frac{1}{b_m (\gamma - 1)} \operatorname{sech}^2(u/2)\, u_x$$

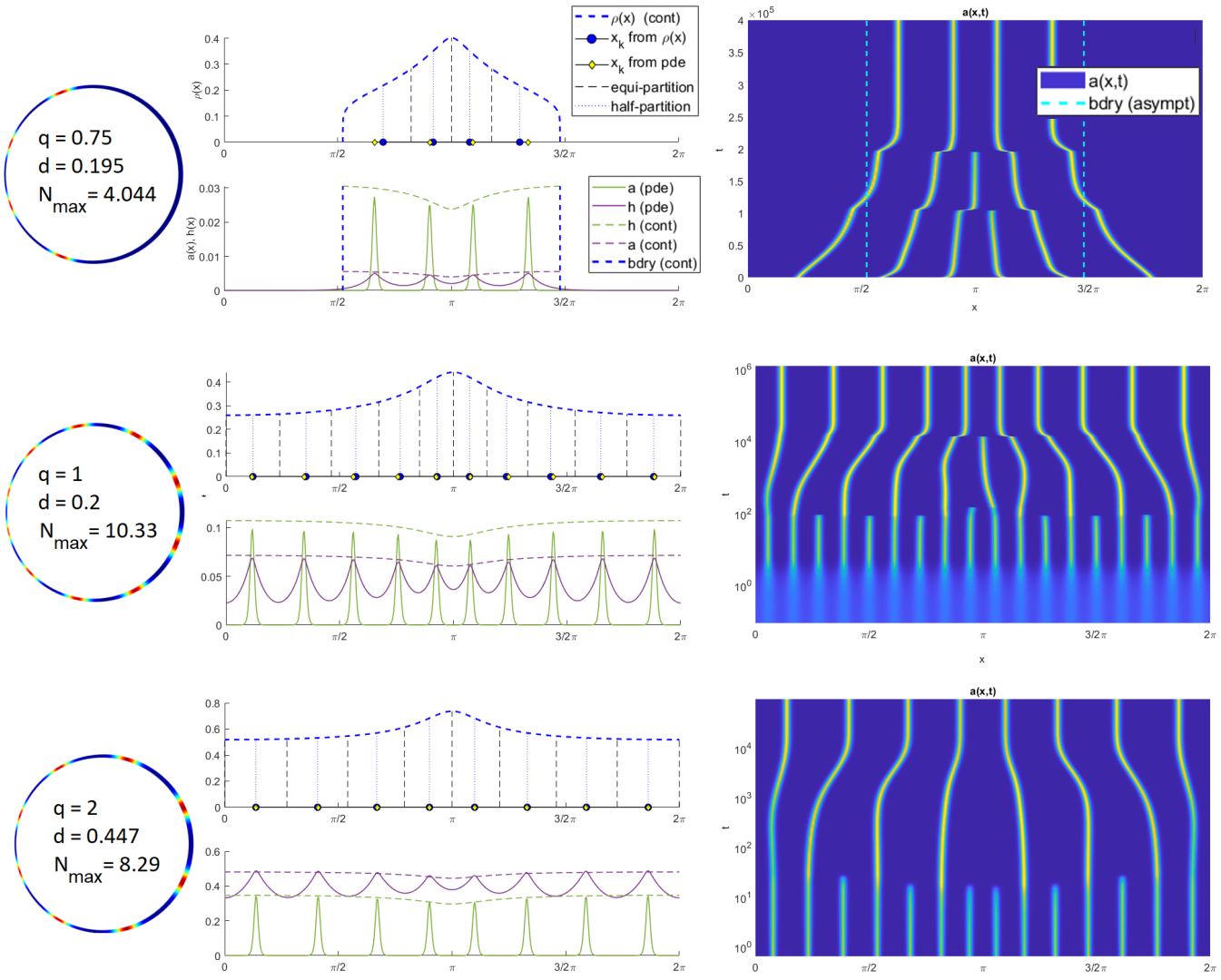

FIG. 4. Simulations of (1) starting with random initial conditions $\varepsilon = 0.018,\ p = 2, m = 2, s = 0$ and with q and d as shown. First column is the colour plot the eventual equilibrium state of $a(x)$. Second column shows the comparison of the steady state along the outer boundary with the continuum limit of many spikes as well as the equilibrium state profile as given by Proposition 3.1. Third column shows the time-space plot along the outer boundary of $a(x,t)$ as well as the cluster radius in the case of $q = 0.75$ as given in Figure 3(e).

so that

$$\frac{1}{V_k}\sum V_j^{\gamma} G_x \sim \frac{u_x}{b_m} F_1 + \frac{\beta}{b_m} F_2$$

where

$$F_1 = \frac{u}{2}\left\{\frac{\gamma}{\gamma-1}\operatorname{sech}^2(u/2)\sum |l|\, e^{-|l|u} - \tanh(u/2)\sum l^2 e^{-|l|u}\right\},$$
$$F_2 = \frac{1}{2}\tanh(u/2)\left\{\sum (|l|\, u - 1)\, e^{-|l|u}\right\}$$

Using $\sum e^{-|l|u} = \coth(u/2)$, $\sum |l| e^{-|l|u} = -\partial_u \coth(u/2)$ and so on we obtain, after some simplifications,

$$F_1 = u\left(\frac{\frac{\gamma+1}{\gamma-1} - \cosh(u)}{2\sinh^2(u)}\right), \qquad F_2 = \frac{u}{2\sinh(u)} - \frac{1}{2}.$$

The steady state then satisfies $-\alpha(x) - 2\frac{p-1}{q}\left(u_x F_1(u) + \alpha(x) F_2(u)\right) = 0$, or

$$u_x = \alpha(x)\frac{\left(\left(\frac{p-1}{q} - 1\right)\frac{\sinh u}{u} + 1\right)\sinh(u)}{\cosh(u) - \frac{\gamma+1}{\gamma-1}}. \tag{21}$$

This is a separable ODE and determines the effective effective inter-spike distance ud in the limit of large N. We summarize as follows.‘

Proposition 3.1. *Suppose that $N \gg O(1)$ and $Nd \leq O(1)$. Let $x_1 \dots x_N$ be the equilibrium state of (10), sorted in increasing order. Its density distribution is given by $\rho(x) = 1/u(x)$, where $u(x)$ satisfies (21) subject to an integral constraint*

$$\int_D \rho(x)dx = Nd. \tag{22}$$

where D is the support of $\rho(x)$.

Note that the right hand side of (21) has a singularity when $\cosh(u) - \frac{\gamma+1}{\gamma-1}$. As in [28], it is observed numerically that when u is below this critical value, the solution is unstable, and in fact the reduced system (10) does not converge to a steady state. This is summarized as follows.

Proposition 3.2. *Let*

$$u_c := \operatorname{arccosh}\left(\frac{\gamma+1}{\gamma-1}\right), \quad \rho_c := 1/u_c. \tag{23}$$

Any stable *equilibrium solution must satisfy $\rho(x) \leq \rho_c$ or equivalently, $u(x) \geq u_c$ for all x in the support of $\rho(x)$. In particular, the inter-spike distance must be larger than $u_c d$.*

This threshold has simple interpretation in terms of the original model (3): $u_c d$ is the minimum possible distance between the spikes; spikes that are closer than that distance are unstable. Formula (23) generalizes the famous instability thresholds of a homogeneous GM system first derived in [2]. To see the equivalence between u_c and results in [2], consider a homogeneous problem ($\alpha = 0$) on the domain of size L. Then $u_x = 0$ so the density $\rho(x)$ is constant, and (22) yields $\rho(x) = \frac{1}{NdL}$. The instability threshold (23) then becomes $NL = d \operatorname{arccosh}\left(\frac{\gamma+1}{\gamma-1}\right)$. Some algebra shows that this is equivalent to the formula (4.65) in [2]. This equivalence was first observed in [28] for the "standard" case $(p, q, m, s) = (2, 1, 0, 2)$.

Let us now define

Definition 3.3. *We call the density $\rho(x) = 1/u(x)$ "admissable" if $\rho(x) \leq \rho_c$ for all x, where ρ_c is given by (23). We call $\rho(x)$ maximal admissable density, denoted it by $\rho_{\max}(x)$, if $\rho_{\max}(x) \geq \rho(x)$ for any admissable density $\rho(x)$.*

Figure 3(a) shows different possible admissable solutions for $\rho(x)$, all below ρ_c with parameters as specified in the figure. Since $\rho(x)$ solves an ODE whose solution is unique, the different solutions cannot intersect. As such, $\rho_{\max}(x)$ must touch ρ_c at its maximum. To solve (21) we fix initial conditions $u(\pi)$ and then integrate (21) numerically, until either $u(x)$ blows up or entire domain is filled. (in figure 3(c), we took initial conditions $u(0)$ instead of $u(\pi)$, in order to capture solutions supported near $x = 0$). The corresponding value of Nd can then be recovered from (22). The different curves in each subfigure correspond to different initial conditions $u_0 = u(\pi)$ (or $u_0 = u(0)$). Depending on parameters, either $u(x)$ will blow up at some points $x = a, b$ (in which case $\rho(x)$ is compactly supported on $[a, b]$ with $\rho(a) = \rho(b) = 0$), or else the solution $u(x)$ exists on the entire domain of definition ($x \in [0, 2\pi]$ periodic in our example).

In the case of a blowup at $x = a, b$, the density $\rho(x) = 1/u(x)$ is compactly supported on the domain $D = (a, b)$. This happens, for example in Figure 3(a) ($q = 0.7$) for *any* admissable ρ. Due to symmetry of $\alpha(x)$, we find that $D = (\pi - R, \pi + R)$ for some R that depends on the choice of initial conditions $u(\pi)$. In this case, the solution is said to have a *cluster*, with spikes inside D and no spikes outside of D.

Let $R_{\max}$ be the radius of the cluster corresponding to $\rho_{\max}$. Figure 3(d) gives the values of $R_{\max}$ corresponding to $u_{\max}$, as well as $N_{\max}d = \int_D \rho_{\max}(x)dx$, for a given value of q. Note the transition from a cluster to a global solution around $q \approx 0.82$. In the absence of the blowup for u, the spikes are globally distributed throughout $[0, 2\pi]$ and no cluster forms.

When $q = 0.7$, note that as $\rho(\pi)$ is decreased, the corresponding radius R approaches to zero, and Nd defined through (22) also approaches zero. As a consequence, the cluster becomes *localized* near $x = \pi$ as $d \to 0$ (and with fixed N) in this case.

Definition 3.4. *We call N-spike equilibrium a "cluster" solution on (a, b) if the corresponding density $\rho(x)$ is compactly supported on $x \in (a, b)$, that is $u(x)$ blows up (has vertical asymptote) at $x = a, b$. If $u(x)$ is defined on entire domain, we call it a "global" solution.*

An important special case is $q = p - 1$. In this case the blowup is not possible: for large u, equation (21) reduces to $u_x \sim \alpha(x)$ which does not have vertical asymptote. As illustrated in Figure 3(b), the density approaches constant as $Nd \to 0$ in this case (this corresponds to the solution of $u_x \sim \alpha(x)$ subject to initial conditions $u(x_0) = u_0 \gg 1$; the solution is indeed $u(x) \sim u_0 + \int_{x_0}^{x} \alpha(s)ds \sim u_0$).

The situation is very different for $q \neq p - 1$: the cluster solution appears for sufficiently small d, either at $x = \pi$ (if $q < p - 1$) or at $x = 0$ (if $q > p - 1$) as we will now show.

Suppose $\alpha(0) = 0$ and we look for cluster solution localized near $x = 0$, with $\rho(x)$ small (i.e. $u(x)$ big). Assuming $u(x)$ is large and the cluster is near $x = 0$, equation (21) can be written as

$$u_x \sim 2\alpha_1 x e^u/u, \quad u \gg 1, \tag{24}$$

where

$$\alpha_1 := \alpha'(0)\frac{1}{4}\left(\frac{p-1}{q} - 1\right) \tag{25}$$

Assuming $\alpha_1 > 0$, this ODE is integrable and after some algebra, its solution $\rho = 1/u$ is approximated by

$$\rho \sim \frac{1}{-2\log R\alpha_1 - \log\left(1 - \left(\frac{x}{R}\right)^2\right)} \sim \begin{cases} \frac{1}{-2\log R\alpha_1}, & |x| < R \\ 0, & |x| > R \end{cases}. \tag{26}$$

Equation (22) then yields an estimate

$$Nd \sim \frac{R}{-\log R\alpha_1}.$$

More generally, we summarize as follows.

Proposition 3.5. *Supplose that $\alpha'(x_0) = 0$ and let α_1 be as in (25) but with $\alpha'(0)$ replaced by $\alpha'(x_0)$. Moreover suppose that $\alpha_1 > 0$. Then there exists a stable cluster of spikes centered at x_0 of radius $R \ll 1$ having $N \gg 1$ spikes when*

$$d \sim \frac{1}{N}\frac{R}{\log\left(1/(Ra)\right)}. \tag{27}$$

The corresponding spike density inside this cluster asymptotes to (26).

Starting from random initial conditions. The existence of a maximal admissable density $\rho_{\max}(x)$ has implications for coarsening phenomenon widely observed for GM systems. Define

$$N_{\max} := \frac{1}{d}\int \rho_{\max}(x)dx. \tag{28}$$

Given a solution with N spikes corresponding to a density $\rho(x)$, we have that $Nd = \int \rho(x)dx \leq \int \rho_{\max}(x)dx = N_{\max}d$. It follows that an equilibrium state can have at most $N_{\max}$ spikes. However, it is possible to have a quasi-equilibrium state with more than $N_{\max}$ spikes; in this case, coarsening is observed whereby some spikes are gradually eliminated until at most $N_{\max}$ remain. In particular this occurs naturally as a result of a Turing bifurcation when starting with random initial conditions as we illustrate below.

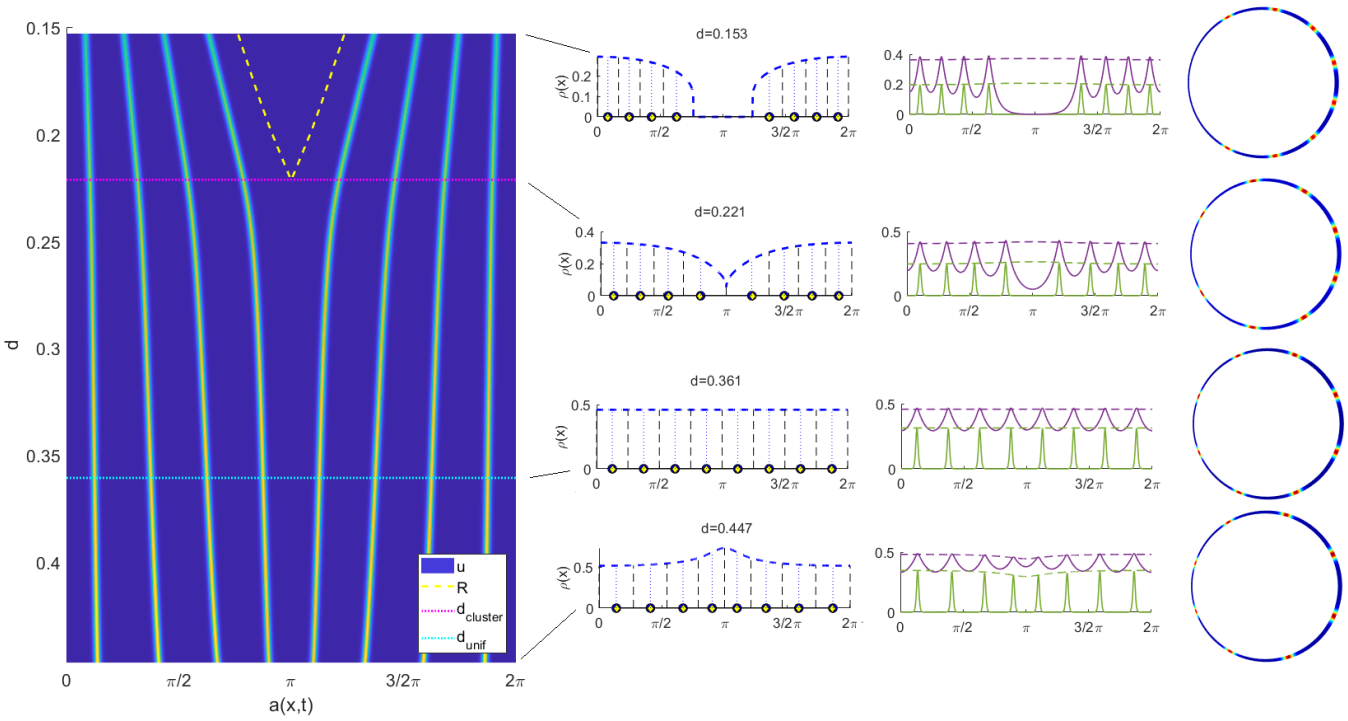

FIG. 5. Simulations of (1) starting with random initial conditions, with $\varepsilon = 0.018$, $p = q = m = 2, s = 0$ and with slowly decreasing d according to $d = 0.447 + 10^{-7}(0.153 - 0.447)t$, $t = 0 \dots 10^7$. Snapshots show direct comparison with continuum density for d as indicated as well as the corresponding steady state. Note that the spike distribution is uniform when $d = 0.361$ (see text); and a cluster starts to form around $d = 0.221$, in full agreement with the theory.

Figure 4 shows the dynamics and the steady state of (1) for three different values of q (either $q < p-1$, $q = p-1$ or $q > p-1$), and starting with initial conditions which consist of small random perturbations off a constant. Turing analysis reveals that the most unstable mode scales like $O(1/\varepsilon)$, and as such, very high-mode instability is triggered. This is followed very quickly by a development of numerous spikes – in fact, more than than the domain can support. As a result, the initial spike pattern undergoes a coarsening process, whereby several spikes are killed in a succession, until $N \sim N_{\max}$. The coarsening process eventually terminates and the pattern converges to an equilibrium configuration. As shown in Figure 4 (first row), when $q = 0.75$, the resulting equilibrium conists of a *cluster* of four spikes, concentrated near the thinnest part of the domain. By contrast, when $q = 1$ or 2, the resulting equilibrium spans an *entire* domain. The number of spikes in each case is is predicted by $N_{\max}$ as given in (28) and indicated in the figure. It agrees very well with actual observations.

Our theory approximates both the maximum number of stable spikes supported by the domain, whether the resulting steady state consists of a cluster of spikes or spikes distributed (non-uniformly) throughout the domain, as well as the actual spike density within the cluster. In all three cases, the resulting equilibrium is well approximated by the continuum limit. This is true even for a relatively small number of spikes ($N = 4$ in Figure 4).

Decreasing d. Figure 5 shows a sequence of admissable densities with $q = 2$. Note that $\rho_{\max}(x)$ is global and has a maximum at $x = \pi$. On the other hand, a smaller $\rho(x)$ forms a cluster around $x = 0$ and has a maximum there. Inbetween, there is a value of d for which the density is constant. This corresponds to a constant solution of (21) which satisfies $\left(\frac{p-1}{q} - 1\right)\frac{\sinh u}{u} + 1 = 0$ or $\frac{\sinh u}{u} = 2$ or $u \approx 2.1773$. The corresponding value of $Nd = \int_0^{2\pi} \frac{1}{2.1773} = 2.8857$. Setting $N = 8$ as in the figure, yields the value of $d = 0.361$. And indeed, the solution is observed to have uniform distribution of spikes at that value as shown in the figure. Similarly, according to the theory, the cluster first appears (near $x = 0$) when $d = 0.221$. As d is further reduced, the cluster radius decreases. Excellent agreement between the theory and the full 2D numerical PDE simulations is observed throughout entire range of d.

Increasing d. Increasing d generally results in a sequence of coarsening thresholds, as illustrated in Figure 6.

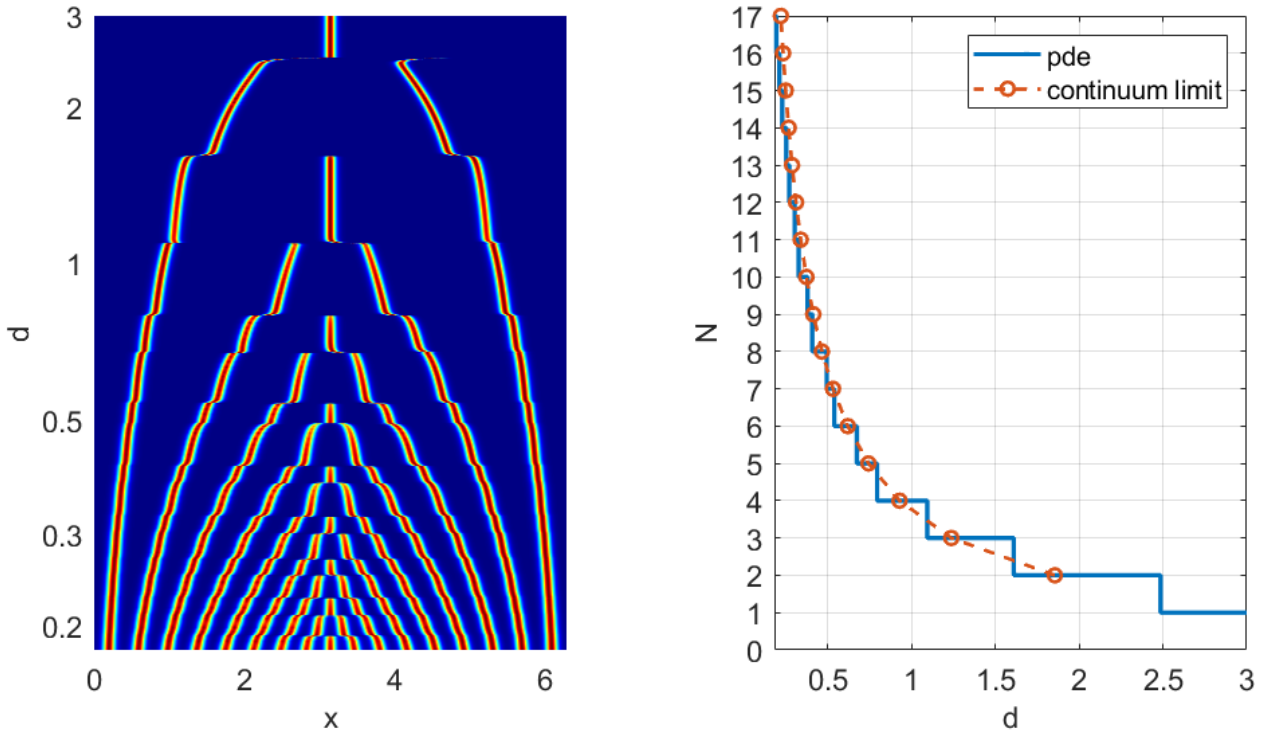

FIG. 6. Simulations of (1) starting with random initial conditions, with $\alpha(x)$ as in (4), $\varepsilon = 0.03$, $p = q = m = 2, s = 0$ and with slowly increasing d according to $d = 0.16 + (3 - 0.0.16)10^{-6}t$, $t = 0 \ldots 10^6$. Left: Full solution to the PDE. Right: N, number of spikes, as a function of d : comparison between the full PDE and the continuum theory (see text)

For parameters in this simulation, we find that $dN_{\max} = \int_0^{2\pi} \rho_{\max}(x)dx = 3.708$. Since $dN_{\max}$ is a fixed constant, increasing d will decrease $N_{\max}$, the maximum possible number of spikes. The location where the coarsening takes place corresponds to the corner in the plot of $\rho_{\max}(x)$, i.e. at $x = \pi$ in this case (c.f. Figure 3). The continuum limit prediction $d \approx 3.708/N_{\max}$ compares well with the full PDE simulation (Figure 6(b)).

4. DISCUSSION

We have described stripe evolution and their equilibrium distributions on thin channels for GM model. We found a rather intricate interplay between exponents p, q, the inhibitor diffusion d, and the domain thickness. Unlike interface-minimizing systems as Allen-Cahn, where the dynamics push the interface to minimize its length and therefore be located at the thinnest part of the channel [38–41], in the GM system it is possible for stripes to be clustered near the maximum of the channel thickness when $q > p - 1$ and d is sufficiently decreased. However even in the case $q > p - 1$, the spike density that arises as a result of a Turing bifurcation is typically higher at the thinner part. It is only when d is sufficiently decreased that the spike density "switches" to the thicker part.

In our analysis and in simulations, we took the domain thickness to be sufficiently small so as to avoid the breakup instability of a stripe into spots [32–36]. For thicker domain (or smaller ε), spots and stripes can coexist, as illustrated in Figure 7. The analysis of this hybrid pattern is left for future work. In particular it would be interesting to construct solutions where the activator is fully two-dimensional, but the inhibitor is is nearly one-dimensional except near the spot. We mention related works [42, 43] which studied the stability and motion of boundary spikes for the GM model.

An interesting "degenerate" case is what happens when a channel is curved but has uniform thickness. Numerical experiments reveal that the stripe will move at a much slower speed in this case, and a rich variety of steady states and equilibria positions is possible; the curvature of the channel seems to play a crucial role. It is an open question to study the motion in this case.

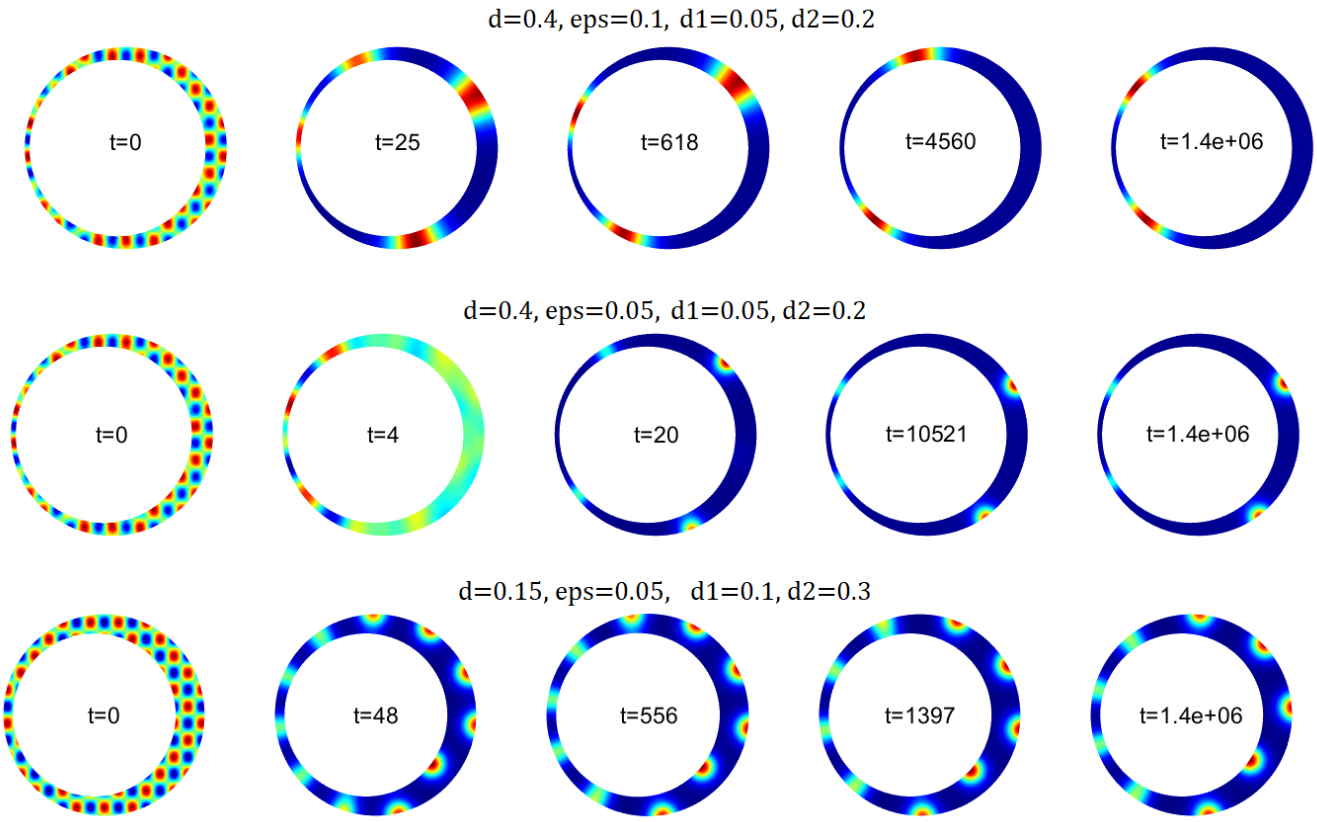

FIG. 7. Coexistence of stripes and spikes. Full simulation of (1) inside a channel whose outer boundary is a unit circle and whose inner boundary is a smaller circle with d_1 and d_2 is the minimum and maximum thickness of the channel. Parameters are $(p, q, m, s) = (2, 0.75, 2, 0)$ with other parameters as indicated. First row: for $\varepsilon = 0.1$, four stripes first appear but only two survive and move towards the thinnest part of the channel. Second row: $\varepsilon = 0.05$, the eventual equilibrium consists of one-dimensional stripes and two-dimensional spots. Third row: Thicker channel and smaller d allows for more spots and stripes to co-exist.

APPENDIX A: EQUATIONS OF MOTION

In this appendix we derive the equations of motion (10) starting with the PDE system (3). Let x_k denote the position of k-th spike. In the inner region near x_k we expand,

$$\begin{aligned} x &= x_k(\varepsilon^2 t) + \varepsilon y, \\ \alpha(x) &= \alpha(x_k) + \alpha'(x_k)\varepsilon y \dots \\ a(x,t) &= U_0(y) + \varepsilon U_1(y) + \dots, \\ h(x,t) &= V_0(y) + \varepsilon V_1(y) + \dots, \end{aligned}$$

Then to leading order we have

$$0 = U_{0yy} - U_0 + \frac{U_0^p}{V_0^q}, \quad 0 = V_{0yy} \tag{29}$$

and at the next order we obtain

$$(-x_k' - \alpha(x_k))\, U_{0y} = U_{1yy} - U_1 + p\frac{U_0^{p-1}U_1}{V_0^q} - q\frac{U_0^p}{V_0^{q+1}}V_1 \tag{30}$$

$$0 = V_{1yy} + U_0^2 \tag{31}$$

Then V_0 is a constant which we denote by $V_0 = V_k$ and therefore U_0 can be written as

$$U_0 = w(y)V_k^{r_1}, \quad r_1 = q/(p-1) \tag{32}$$

where w is the unique ground-state solution to

$$w_{yy} - w + w^p = 0; \quad w'(0) = 0, \quad w \to 0 \text{ as } |y| \to \infty \tag{33}$$

whose explicit solution is given by

$$w(y) = \left(\frac{p+1}{2}\operatorname{sech}^2\left(\frac{p-1}{2}y\right)\right)^{\frac{1}{p-1}}. \tag{34}$$

In the outer region, we write

$$h(x) \sim \sum_{j=1}^{N} S_j G(x, x_j) \tag{35}$$

where G is the Green's function solution to

$$d^2\left(G_{xx} + \alpha(x)G_x\right) - G + \delta(x,y) = 0. \tag{36}$$

The weights S_j are computed as

$$S_j = \int_{x_j-}^{x_j^+} \frac{u^m(x)}{h^s(x)}\frac{1}{\varepsilon}dx \sim V_j^{mr_1-s}\int w^m dy.$$

Matching inner and outer region we have $V_k \sim h(x_k)$ so that

$$S_k \sim V_k^{mr_1-s}b_m, \quad \text{where} \quad b_m = \int w^m dy, \tag{37}$$

$$V_k \sim \sum_{j=1}^{N} S_j G(x_k, x_j) \tag{38}$$

Finally we formulate the solvability condition to determine x_k. Multiplying (30) by U_{0y} and integrating by parts, we then obtain

$$\left(-x_k' - \alpha\left(x_k\right)\right)\int U_{0y}^2 = -\int qU_{0y}\frac{U_0^p}{V_0^{q+1}}V_1 \tag{39}$$

$$0 = V_{1yy} + U_0^m/V_0^s \tag{40}$$

We compute

$$\begin{aligned} -\int qU_{0y}\frac{U_0^p}{V_0^{q+1}}V_1 &= \frac{q}{V_0^{q+1}}\frac{1}{p+1}\int U_0^{p+1}V_{1y} \\ &\sim \frac{q}{p+1}V_0^{-q-1+r_1(p+1)}\left\langle h_x\right\rangle_k \int w^{P+1} \end{aligned} \tag{41}$$

where $\left\langle h_x\right\rangle_k$ denotes the average of the slopes in the outer regions for $h(x)$, $\left\langle h_x\right\rangle_k := \frac{h_x(x_k^+)+h_x(x_k^-)}{2}$.

Finally, we multiply (33) by w' or w and then integrate to obtain the identities

$$\begin{aligned} 0 &= -\int w_y^2 - \int w^2 + \int w^{p+1} \\ 0 &= \frac{1}{2}\int w_y^2 - \frac{1}{2}\int w^2 + \frac{1}{p+1}\int w^{p+1} \end{aligned}$$

so that

$$\frac{\int w^{p+1}}{\int w_y^2} = 2\frac{p+1}{p-1};$$

this yields

$$x_k'(\varepsilon^2 t) = -\alpha\left(x_k\right) + 2\frac{q}{p-1} v_k^{-1} \left\langle v_x \right\rangle_k . \tag{42}$$

Finally we have

$$\left\langle h_x \right\rangle_k = b_m \sum_{j=1}^{N} V_k^{mr_1 - s} G_x(x_k, x_j). \tag{43}$$

where $G_x(x_k, x_k) = \lim_{\varepsilon \to 0} \frac{G_x(x_k+\varepsilon, x_k) + G_x(x_k-\varepsilon, x_k)}{2}$. Substituting (43) into (42) yields the system (10).

For a single spike, this reduces to:

$$x_0'(\varepsilon^2 t) = -\alpha\left(x_0\right) - 2\frac{q}{p-1}\frac{G_x(x_0, x_0)}{G(x_0, x_0)}. \tag{44}$$

Finally for small D, this simplifies (see Appendix B) to

$$x_0'(\varepsilon^2 t) = \left(-1 + \frac{q}{p-1}\right)\alpha(x_0). \tag{45}$$

APPENDIX B: GREEN'S FUNCTION AND WKB THEORY

We are looking for solution to the equation

$$d^2\left(G_{xx} + a(x) G_x\right) - G = -\delta(x-\xi); \qquad d \ll 1.$$

We use the standard WKB anzatz:

$$\phi'^2 = 1; \ \frac{1}{Y}\left(Y^2 \phi'\right)' + Y\phi'\beta = 0.$$

Since we require decay at infinity, we take $\phi' = -\operatorname{sign}(x-\xi)$ and equation for Y yields

$$Y = C \exp\left(-\frac{1}{2}\int_{\xi}^{x} \alpha\left(s\right) ds\right).$$

Applying the jump condition $d^2 G_x|_{\xi^-}^{\xi^+} = -1$; then yeilds

$$G(x,\xi) = \frac{1}{2d}\exp\left(-\frac{1}{2}\int_{\xi}^{x}\alpha\left(s\right)ds\right)\exp\left(-\frac{|x-\xi|}{d}\right).$$

In particular we have:

$$G(\xi,\xi) = \frac{1}{2d} \tag{46}$$

$$G_x(\xi,\xi) = \frac{G_x(\xi^+,\xi) + G_x(\xi^-,\xi)}{2} = -\frac{\alpha\left(\xi\right)}{4d}; \tag{47}$$

and two-order for $x = \xi + dy$ yields

$$G(\xi + dy, \xi) \sim \frac{1}{2d} e^{-|y|} - \frac{\alpha\left(\xi\right)}{4} y e^{-|y|}; \tag{48}$$

$$G_x(\xi + dy, \xi) \sim -\frac{1}{2d^2}\operatorname{sign} y e^{-|y|} + d\frac{\alpha(\xi)}{4d}\left(|y| - 1\right)e^{-|y|} \tag{49}$$

APPENDIX C: THIN CHANNEL REDUCTION

Reduction to 1D. We now show the derivation of (2). Assume a channel has cross-sectional area $A(s)$, where s is the acrlength coordinate along one of the boundaries. We will show that the general equation $\Delta u + F = 0$ inside the channel with Neumann boundary conditions reduces to $u_{ss} + \frac{A'(s)}{A(s)} u_s + F = 0$. Here, u is a multi-component variable, and $F = F(u, u_t)$ is the remaining nonlinearity.

In curvilinear coordinates, Laplacian is written as:

$$\Delta u = u_{\eta\eta} - \frac{\kappa}{1-\kappa\eta} u_\eta + \frac{1}{1-\kappa\eta} \left(\frac{1}{1-\kappa\eta} u_s \right)_s \tag{50}$$

Here, s is the arclength coordinate along a boundary, and η is the coordinate ornonormal to s, pointing inside the domain, and $\kappa = \kappa(s, \eta)$ is the curvature along the curve $s = const.$ as illustrated in the following figure:

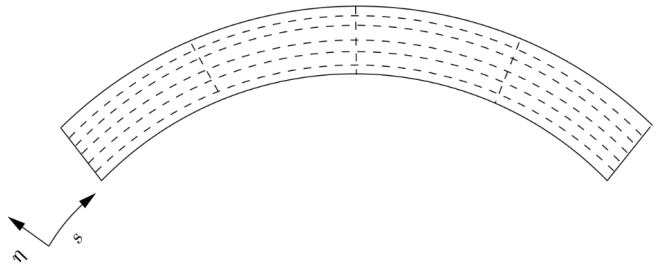

We have:

$$\kappa(s, \eta) = \frac{\kappa_0(s)}{1 + \eta\kappa_0(s)}$$

so that (50) becomes

$$\Delta u = u_{\eta\eta} - \kappa_0 u_\eta + (1 + \eta\kappa_0) \left((1 + \eta\kappa_0) u_s \right)_s .$$

The boundary condition $\partial_n u = 0$ at $\eta = \delta f(s)$ becomes, to leading order:

$$\delta f'(s) u_s \sim u_\eta \text{ at } \eta = \delta f(s) \tag{51}$$

Rescale $\eta = z\delta$. We have:

$$\Delta u = \frac{1}{\delta^2} u_{zz} - \frac{1}{\delta} \kappa_0 u_z + (1 + z\delta\kappa_0)^2 u_{ss} + (1 + z\delta\kappa_0) z\delta\kappa_0'(s) u_s$$

and (51) yields

$$u_z \sim \delta^2 f'(s) u_s \text{ at } z = f(s).$$

The equation is $\Delta u + F = 0$. Integrate in the $z = 0 \dots f(s)$ to obtain, to leading order,

$$f'(s) u_s + f(s) u_{ss} + f(s) F = 0$$

or $u_{ss} + \frac{f'(s)}{f(s)} u_s + F = 0$.

Annular region. Consider an annular domain as in 1 where the outer boundary is a unit circle and the inner boundary is circle such that minimum and maximum distance from the outer boundary is m and κm, respectively. Assume without loss of generality that the distance is at the minimum at $\theta = \pi$ and is maximum at $\theta = 0$. The length of cross-section corresponding to angle θ is given by $L(\theta) = \left| c + re^{i\theta} - e^{i\theta} \right|$, where $r = 1 - \frac{m}{2}(1 + \kappa)$ and $c = 1 - \kappa m - r = m\left(\frac{1}{2} - \frac{\kappa}{2}\right)$. We we find that:

$$L(\theta) = \frac{m}{4} \left(1 + \kappa^2 + \left(\kappa^2 - 1 \right) \cos\theta \right)^{1/2}$$

so that $\alpha = \beta = L'/L$:

$$\alpha = \beta = \frac{1}{2}\frac{-\left(\kappa^2 - 1\right)\sin\theta}{1 + \kappa^2 + (\kappa^2 - 1)\cos\theta};$$

here, κ is the ratio of maximum versus minimum.

[1] A. Gierer, H. Meinhardt, A theory of biological pattern formation, Kybernetik 12 (1) (1972) 30–39.
[2] D. Iron, M. J. Ward, J. Wei, The stability of spike solutions to the one-dimensional gierer–meinhardt model, Physica D: Nonlinear Phenomena 150 (1) (2001) 25–62.
[3] J. D. Murray, Mathematical Biology. II Spatial Models and Biomedical Applications {Interdisciplinary Applied Mathematics V. 18}, Springer-Verlag New York Incorporated, 2001.
[4] J. Wei, M. Winter, Mathematical aspects of pattern formation in biological systems, Vol. 189, Springer Science & Business Media, 2013.
[5] W. N. Reynolds, S. Ponce-Dawson, J. E. Pearson, Self-replicating spots in reaction-diffusion systems, Physical Review E 56 (1) (1997) 185.
[6] A. Doelman, T. J. Kaper, P. A. Zegeling, Pattern formation in the one-dimensional gray-scott model, Nonlinearity 10 (2) (1997) 523.
[7] Theory of domain patterns in systems with long-range interactions of coulomb type, Physical Review E 66 (6) (2002) 066108.
[8] Y. Nishiura, D. Ueyama, Spatio-temporal chaos for the gray–scott model, Physica D: Nonlinear Phenomena 150 (3) (2001) 137–162.
[9] T. Kolokolnikov, M. J. Ward, J. Wei, The existence and stability of spike equilibria in the one-dimensional gray–scott model: The low feed-rate regime, Studies in Applied Mathematics 115 (1) (2005) 21–71.
[10] D. L. Benson, P. K. Maini, J. A. Sherratt, Unravelling the turing bifurcation using spatially varying diffusion coefficients, Journal of Mathematical Biology 37 (5) (1998) 381–417.
[11] D. Iron, J. Wei, M. Winter, Stability analysis of turing patterns generated by the schnakenberg model, Journal of mathematical biology 49 (2004) 358–390.
[12] J. Wei, M. Winter, Flow-distributed spikes for schnakenberg kinetics, Journal of mathematical biology 64 (2012) 211–254.
[13] C. A. Klausmeier, Regular and irregular patterns in semiarid vegetation, Science 284 (5421) (1999) 1826–1828.
[14] J. A. Sherratt, An analysis of vegetation stripe formation in semi-arid landscapes, Journal of mathematical biology 51 (2) (2005) 183–197.
[15] J. A. Sherratt, G. J. Lord, Nonlinear dynamics and pattern bifurcations in a model for vegetation stripes in semi-arid environments, Theoretical population biology 71 (1) (2007) 1–11.
[16] Y. Chen, T. Kolokolnikov, J. Tzou, C. Gai, Patterned vegetation, tipping points, and the rate of climate change, European Journal of Applied Mathematics 26 (06) (2015) 945–958.
[17] C. Gai, T. Kolokolnikov, Resource-mediated competition between two plant species with different rates of water intake, SIAM Journal on Applied Mathematics 83 (2) (2023) 576–602.
[18] F. Al Saadi, A. Champneys, C. Gai, T. Kolokolnikov, Spikes and localised patterns for a novel schnakenberg model in the semi-strong interaction regime, European Journal of Applied Mathematics 33 (1) (2022) 133–152.
[19] M. B. Short, M. R. D'ORSOGNA, V. B. Pasour, G. E. Tita, P. J. Brantingham, A. L. Bertozzi, L. B. Chayes, A statistical model of criminal behavior, Mathematical Models and Methods in Applied Sciences 18 (supp01) (2008) 1249–1267.
[20] J. R. Zipkin, M. B. Short, A. L. Bertozzi, Cops on the dots in a mathematical model of urban crime and police response, to appear, DCDS-S (supplement) (2014).
[21] T. Kolokolnikov, M. J. Ward, J. Wei, The stability of steady-state hot-spot patterns for a reaction-diffusion model of urban crime., Discrete & Continuous Dynamical Systems-Series B 19 (5) (2014).
[22] S. Chaturapruek, J. Breslau, D. Yazdi, T. Kolokolnikov, S. G. McCalla, Crime modeling with lévy flights, SIAM Journal on Applied Mathematics 73 (4) (2013) 1703–1720.
[23] S. Kondo, R. Asai, et al., A reaction-diffusion wave on the skin of the marine angelfish pomacanthus, Nature 376 (6543) (1995) 765–768.
[24] R. Barrio, C. Varea, J. Aragón, P. Maini, A two-dimensional numerical study of spatial pattern formation in interacting turing systems, Bulletin of mathematical biology 61 (3) (1999) 483–505.
[25] P. K. Maini, T. E. Woolley, R. E. Baker, E. A. Gaffney, S. S. Lee, Turing's model for biological pattern formation and the robustness problem, Interface focus (2012) rsfs20110113.
[26] J. Wei, M. Winter, Spikes for the two-dimensional gierer-meinhardt system: the weak coupling case, Journal of Nonlinear Science 11 (2001) 415–458.
[27] J. Wei, M. Winter, W. Yang, Stable spike clusters for the precursor gierer–meinhardt system in r^ 2 r 2, Calculus of Variations and Partial Differential Equations 56 (2017) 1–40.
[28] T. Kolokolnikov, S. Xie, Spike density distribution for the gierer–meinhardt model with precursor, Physica D: Nonlinear Phenomena 402 (2020) 132247.

[29] T. Kolokolnikov, J. Wei, Hexagonal spike clusters for some pde's in 2d, Discrete and Continuous Dynamical Systems-B 25 (10) (2020) 4057–4070.
[30] K. M. Page, P. K. Maini, N. A. Monk, Complex pattern formation in reaction–diffusion systems with spatially varying parameters, Physica D: Nonlinear Phenomena 202 (1) (2005) 95–115.
[31] T. Kolokolnikov, J. Wei, Pattern formation in a reaction-diffusion system with space-dependent feed rate, SIAM Review 60 (3) (2018) 626–645.
[32] A. Doelman, H. van der Ploeg, Homoclinic stripe patterns, SIAM Journal on Applied Dynamical Systems 1 (1) (2002) 65–104.
[33] D. S. Morgan, T. J. Kaper, Axisymmetric ring solutions of the 2d gray–scott model and their destabilization into spots, Physica D: Nonlinear Phenomena 192 (1-2) (2004) 33–62.
[34] T. Kolokolnikov, W. Sun, M. Ward, J. Wei, The stability of a stripe for the gierer–meinhardt model and the effect of saturation, SIAM Journal on Applied Dynamical Systems 5 (2) (2006) 313–363.
[35] T. Kolokolnikov, M. J. Ward, J. Wei, Zigzag and breakup instabilities of stripes and rings in the two-dimensional gray–scott model, Studies in Applied Mathematics 116 (1) (2006) 35–95.
[36] T. Kolokolnikov, M. Ward, J. Tzou, J. Wei, Stabilizing a homoclinic stripe, Philosophical Transactions of the Royal Society A: Mathematical, Physical and Engineering Sciences 376 (2135) (2018) 20180110.
[37] T. Kolokolnikov, M. J. Ward, Bifurcation of spike equilibria in the near-shadow gierer-meinhardt model, Discrete and Continuous Dynamical Systems-B 4 (4) (2004) 1033–1064.
[38] R. V. Kohn, P. Sternberg, Local minimisers and singular perturbations, Proceedings of the Royal Society of Edinburgh Section A: Mathematics 111 (1-2) (1989) 69–84.
[39] X. Chen, Generation and propagation of interfaces for reaction-diffusion equations, Journal of Differential equations 96 (1) (1992) 116–141.
[40] T. Ilmanen, Convergence of the allen-cahn equation to brakke's motion by mean curvature, Journal of Differential Geometry 38 (2) (1993) 417–461.
[41] D. Iron, T. Kolokolonikov, J. Rumsey, J. Wei, Stability of curved interfaces in the perturbed two-dimensional allen–cahn system, SIAM Journal on Applied Mathematics 69 (5) (2009) 1228–1243.
[42] W. Ao, J. Wei, M. Winter, Stable boundary spike clusters for the two-dimensional gierer–meinhardt system, Journal de Mathématiques Pures et Appliquées 121 (2019) 1–46.
[43] The dynamics of boundary spikes for a nonlocal reaction-diffusion model, European Journal of Applied Mathematics 11 (5) (2000) 491–514.